Microwave Power Limits of AlGaN/GaN HEMTs Under Pulsed-Bias Conditions

Bruce M. Green, *Member, IEEE*, Vinayak Tilak, Valery S. Kaper, *Student Member, IEEE*, Joseph A. Smart, James R. Shealy, and Lester F. Eastman, *Life Fellow, IEEE*

***Abstract*—Dynamic loadline analysis illustrating the microwave performance limits of state-of-the-art AlGaN/GaN high electron-mobility transistors (HEMTs) under pulsed RF biasing and drive conditions are presented. Calculation of dynamic loadlines concurrent with load–pull measurements show the increase of the device RF knee voltage with increasing drain voltage as the cause of reduced output power-added efficiency (PAE) at high drain biases. In this study, an 8-GHz saturated output power of 14.1 W (9.4 W/mm) is achieved on a 1500 $\times$ 0.25 $\times$ μm^2 AlGaN/GaN HEMT at a pulsed drain bias of $V_D = 40$ V. The pulsed-bias conditions considered here preclude device self-heating as a mechanism responsible for the lower than expected output power and decrease in PAE with increasing drain bias. These data suggest electron trapping associated with the surface of the device between the gate and drain as the mechanism that limit the ultimate power, PAE, and linearity of AlGaN/GaN HEMTs.**

***Index Terms*—Dynamic loadline, gallium nitride, high electron-mobility transistor (HEMT), silicon carbide.**

I. Introduction

ALUMINUM gallium nitride/gallium nitride (AlGaN/GaN) high electron mobility transistor (HEMT) technology has established itself as a leading competitor for future high-frequency high-power microwave applications. The advantages of this material system for these applications arise from its wide bandgap of 3.4 eV coupled with its relatively high saturated electron velocity of 1.5–2 $\times$ 10^7 cm/s [1]. Published reports for these devices demonstrate unprecedented continuous wave (CW) power densities for GaN HEMTs on sapphire and SiC substrates [2]–[5]. These reports clearly show the potential of GaN-based devices for high-frequency high-power applications. However, few reports illustrate what aspects of this developing technology (e.g., self-heating, dc–RF dispersion, breakdown, etc.) still limit the electrical performance of the devices. In the past, dynamic loadline analysis has been used to study the CW performance of GaAs MESFETs and pseudomorphic high electron-mobility transistors (pHEMTs) [6], [7] and AlGaN/GaN HEMTs [2]. However, until now, this technique has not been used to study the pulsed RF performance of AlGaN/GaN HEMTs.

This paper explores the electrical limits of state-of-the art AlGaN/GaN HEMTs under pulsed-bias conditions using I_D–V_D plane dynamic loadline analysis. It first gives a brief description of the device technology followed by a description of a load–pull system and technique used to extract dynamic loadlines at the device plane. The effect of trap-related dc–RF current dispersion, input power drive, and bias voltage on power density, power-added efficiency (PAE), and saturation characteristics are explored based on the determination of drain current dynamic loadlines measured at 8 GHz. These measured dynamic loadlines clearly elucidate how the measured RF response correlates with the static I_D–V_D curves as a measure of the degree of dc–RF dispersion. These measured data suggest a bias-dependent device on resistance as the mechanism for the observed premature gain compression. A pulsed power of 14.1 W (9.4 W/mm, 43% PAE) was obtained from a single 1500 $\times$ 0.25 $\times$ μm^2 device at $V_D = 40$ V, demonstrating the tremendous electronic potential of the device technology. However, at this relatively high drain bias, the minimum RF voltage is approximately 12 V above the measured dc knee voltage. This suggests that, with future improvements in the technology, AlGaN/GaN-based transistors have the potential to deliver even higher power density, PAE, and linearity.

II. Device Technology

The devices in this study are grown by organo-metallic vapor phase epitaxy on 330-μm SiC substrates using the process described in [8] and [9]. For these devices, the AlGaN barrier thickness is 200 Å and the aluminum mole fraction is 0.33. The material is undoped and relies solely on spontaneous and piezoelectric polarization for provision of the channel charge [8]. As shown in [2] and [11], surface passivation of the devices by an Si_3N_4 layer is essential for high power density operation. The devices considered in this study were passivated using a 1000-Å Si_3N_4 layer [10]. Small periphery devices fabricated using this process have achieved >10-W/mm CW power densities at 10 GHz [2]. The 10 $\times$ 150 $\times$ 0.25 μm^2 HEMTs that are used in this study have a gate-to-gate pitch of 50 μm. Two-finger 2 $\times$ 125 $\times$ 0.25 μm^2 devices from the same wafer as this device have a maximum current of 1.3 A/mm and an extrinsic f_τ of 41 GHz.

Manuscript received April 4, 2002. This work was supported by the Office on Naval Research under the Multiuniversity Research Initiative Contract N00014-96-1-1223.

B. M. Green was with the School of Electrical and Computer Engineering, Cornell University, Ithaca, NY14853 USA. He is now with the Semiconductor Products Sector, Motorola, Tempe, AZ 85284 USA (e-mail: bruce_green@ieee.org).

V. Tilak was with the School of Electrical and Computer Engineering, Cornell University, Ithaca, NY 14853 USA. He is now with the Central Research and Development Laboratories, General Electric, Niskayuna, NY 12304 USA.

V. S. Kaper, J. R. Shealy, and L. F. Eastman are with the School of Electrical and Computer Engineering, Cornell University, Ithaca, NY 14853 USA.

J. A. Smart was with the School of Electrical and Computer Engineering, Cornell University, Ithaca, NY 14853 USA. He is now with RF Micro Devices, Charlotte, NC 27409-9421 USA.

Digital Object Identifier 10.1109/TMTT.2002.807680

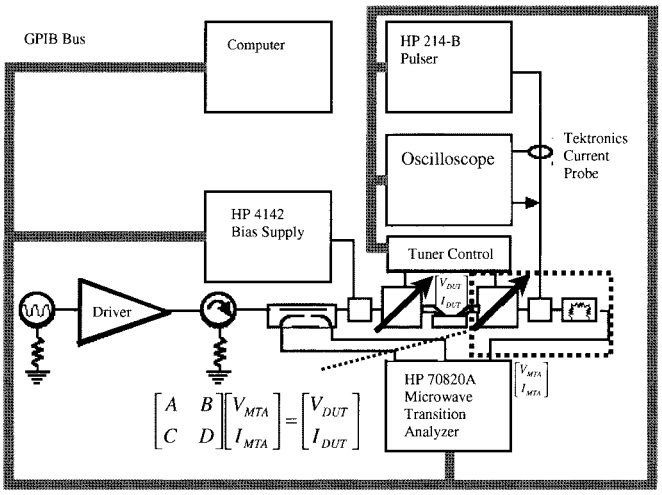

Fig. 1. Diagram of pulsed load–pull system used for the determination of pulsed dynamic loadlines.

III. Measurement Systemand Data Analysis

Since it was desired to understand the electrical limits of the device in the absence of self-heating effects, the pulsed RF load–pull system of Fig. 1 was realized. Pulses with widths down to 100 nS are supplied through the drain bias tee. A pulsed RF input signal is supplied by controlling the synthesized signal source with the microwave transition analyzer (MTA). In addition, the MTA also sends a trigger signal to the HP 214 B pulse generator to synchronize the drain bias with the RF input pulse. The gate bias is held constant using a dc power supply. All of the experimental data presented here use drain-bias pulsewidths of 500 nS with a 1% duty cycle. These short pulse lengths and duty cycles prevent self-heating of the device when in operation.

The determination of the drain I_D–V_D plane dynamic loadline produced by the device is accomplished by using the channels of the Hewlett-Packard 708120A MTA, shown schematically in Fig. 1, as the power sensors of a Maury load–pull system. During the course of a microwave measurement, the voltage waveform read by the MTA is transferred from the MTA to the controlling personal computer (PC). The rms power is determined by the averaging of up to 100 power readings by the MTA. In this way, the slight jitter caused by the pulsed RF measurement conditions is minimized. Agreement between this method of measuring the rms power and the rms power determined by taking the mean of $p_{\rm DUT}(t) = v_{\rm DUT}(t) i_{\rm DUT}(t)$ is typically within 0.3 dB. The calculation of $v_{\rm DUT}(t)$ and $i_{\rm DUT}(t)$ is accomplished via Fourier analysis of $v_{\rm MTA}(t)$, as explained below.

The determination of $v_{\rm DUT}(t)$ and $i_{\rm DUT}(t)$ is accomplished using the $ABCD$ parameters of the output circuit that includes all of the passive components between the DUT and the input port of the MTA. To this end, the probes, tuner, bias tee, attenuator, and all intervening cables are characterized at the fundamental frequency, as well as at the desired number of harmonic frequencies. The work presented here represents the nonlinear waveforms produced by the device using the Fourier components at the fundamental frequency f_0 and two additional harmonic frequencies at $2f_0$ and $3f_0$.

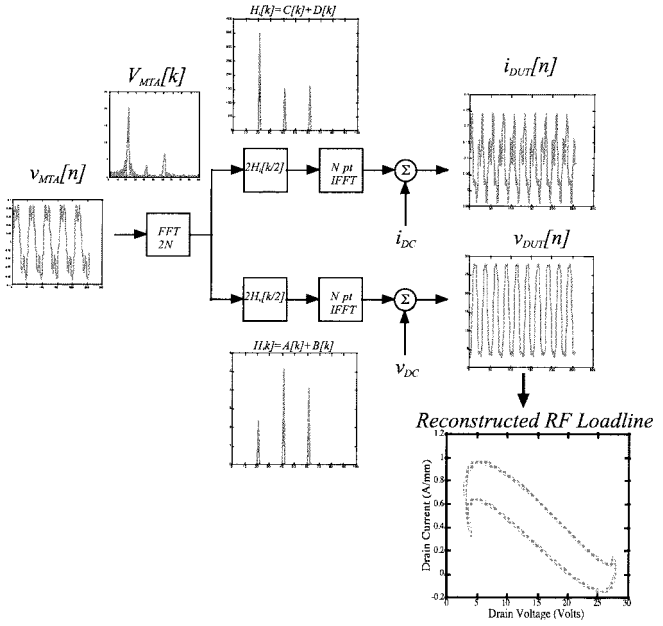

Fig. 2. Block diagram describing signal processing of MTA data for the construction of dynamic loadlines.

The frequency-domain relation between the voltage read at the MTA and the voltage and current at the device probe pads $V_{\rm DUT}(f)$ and $I_{\rm DUT}(f)$ is given by

$$\begin{bmatrix} V_{\rm DUT}(f) \\ I_{\rm DUT}(f) \end{bmatrix} = \begin{bmatrix} A(f) & B(f) \\ C(f) & D(f) \end{bmatrix} \begin{bmatrix} V_{\rm MTA}(f) \\ I_{\rm MTA}(f) \end{bmatrix} \tag{1}$$

where $V_{\rm MTA}(f)$ is the frequency domain representation of $v_{\rm MTA}(t)$ and $I_{\rm MTA}(f) = V_{\rm MTA}(f)/Z_0$. The $ABCD$ parameters of the output circuit are determined from its measured S-parameters using a standard conversion [12].

While the $ABCD$ parameters of the passive network between the DUT plane and MTA are measured using small-signal techniques, by considering the $ABCD$ parameters at the fundamental and harmonic frequencies, the large-signal, nonlinear drain current, and voltage waveforms may be reproduced using Fourier analysis.

In order to implement the computation of (1) using a digital computer, a conjugate-symmetric frequency-domain representation of the $ABCD$-parameters is required. Using this representation of the $ABCD$-parameters, the voltage and current at the device plane are computed using (1), as pictured schematically in Fig. 2. In reality, all of the measured waveform data are discrete time sequences, Therefore, the discrete time and frequency indexes n and k are used to describe the processing of the data in this figure. The multirate signal-processing algorithm of Fig. 2, based on the DFT of $v_{\rm MTA}[n]$ via a fast Fourier transform (FFT) computation, is then used to obtain $v_{\rm DUT}[n]$ and $i_{\rm DUT}[n]$, the sampled versions of $v_{\rm DUT}(t)$ and $i_{\rm DUT}(t)$.

IV. Impact of RF Knee Voltage on Device Saturation Characteristics

A strong motivation for using AlGaN/GaN HEMTs in many applications is the potential for greater RF power density for a

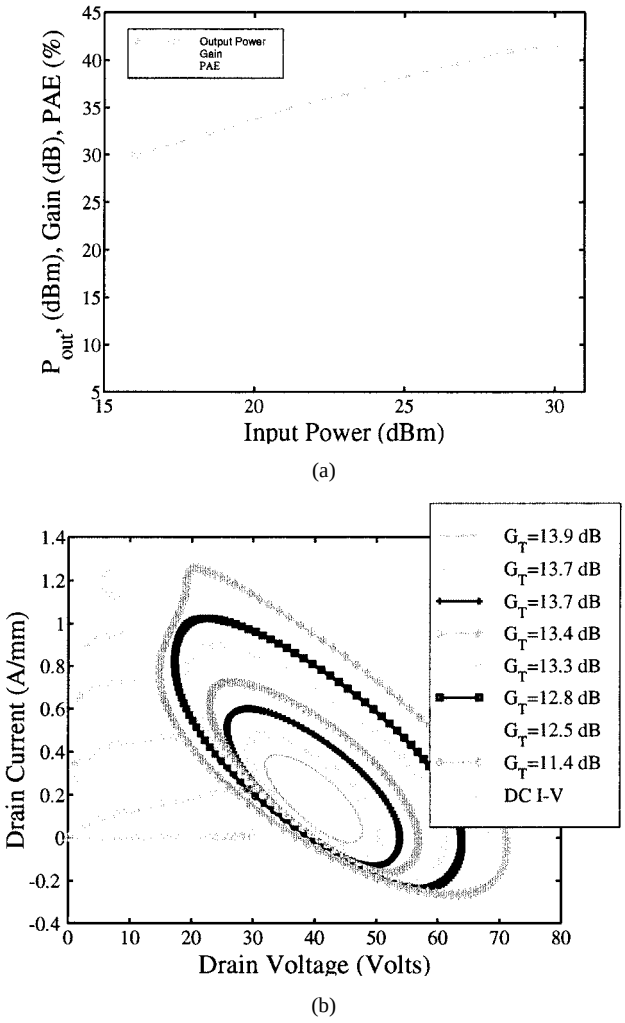

Fig. 3. Measured: (a) saturation characteristics and (b) computed dynamic loadlines for $10 \times 150 \times 0.25$ μm^2 AlGaN/GaN HEMT at $VD = 40$ V, $VG = -3.75$ V under pulsed RF measurement conditions at 8 GHz as a function of drive (I–V curves are measured on $2 \times 150 \times 0.25$ μm^2 HEMT from same wafer).

given linearity due to the higher power at which the 1-dB gain compression point $P_{1\,\mathrm{dB}}$ occurs. As shown in [13], $P_{1\,\mathrm{dB}}$ is a reasonably good indicator of a device's third-order intercept point. Fig. 3(a) shows saturation characteristics for a 1.5-mm AlGaN/GaN HEMT at a pulsed bias of $V_D = 40$ V. For this device, the 1-dB compression power density is 8.4 W/mm (12.6 W total, 36% PAE). As can be seen from this figure, a saturated power density of 9.4 W/mm (14.1 total, 43% PAE) occurs at 2.5-dB compression. Fig. 3(b) gives further insight into the mechanism of the premature gain compression. This figure shows the evolution of the dynamic loadlines during ~2-dB steps and compares them to measured dc I–V characteristics of an adjacent $2 \times 150 \times 0.25$ μm^2 HEMT with identical threshold and on-resistance characteristics as the larger device. Here, a smaller device from the same wafer was used to measure the dc characteristics to avoid excessive self-heating during the measurement. From these data, one can see that the 1-dB compression point occurs just prior to visible distortion of the loadline. At 2.5-dB compression, the loadline is significantly distorted. Fourier analysis of the measured time-domain signal at 2.5-dB compression (14.1 W out) shows that the signal at the second and third harmonics is 22 and 23 dB below the fundamental frequency power, respectively. From the graph, it can be seen that the RF knee voltage is approximately 12 V. Therefore, one would expect less premature gain compression if the dc knee voltage of approximately 4 V could be achieved during microwave operation at this bias point. This increase in knee voltage during RF operation is a product of the lengthening of the gate–edge depletion region with bias, as will be discussed in Section V.

V. Effect of Drain Bias on Power and Efficiency

The large off-state breakdown voltage of the AlGaN/GaN HEMTs considered in this paper (≈70 V) allows the use of bias voltages beyond 30 V for X-band operation. The maximum allowable bias centers the operating point in between the RF knee voltage V_{knee} and the off-state breakdown voltage V_{BD} and is given by

$$V_D < (V_{\mathrm{BD}} + V_{\mathrm{knee}})/2. \tag{2}$$

At first glance, one would suppose that the benefit of a large bias voltage would be an increased PAE (η_A) due to a larger voltage swing compared to the knee voltage. A class-B approximation to the PAE, calculated from resistive loadlines, takes the form [14]

$$\eta_A \approx \frac{\pi}{4} \frac{(\pi - 1)R_{\mathrm{load}}}{(\pi - 1)R_{\mathrm{load}} + \pi R_{\mathrm{on}}} \left(1 - \frac{1}{G}\right). \tag{3}$$

This expression shows that, for a constant load impedance, the PAE should remain constant provided that the on resistance R_{on} does not increase. If, however, the load impedance is held constant and R_{on} increases with increasing V_D, the PAE will decrease. Here, it is assumed that the linear portion of the I_D–V_D characteristics, not the full channel current, limits the on-state portion of the loadline.

The trend of lower PAE with increased drain bias is seen in the experimental data of Fig. 4. As can be seen from Fig. 4(a), while the output power rises with bias (in this case, from 4 W at $V_D = 15$ V to 14.1 W at $V_D = 40$ V), the PAE in Fig. 4(b) stays relatively constant at approximately 50% until it falls to 43% at $V_D = 40$ V. A comparison of the measured 8-GHz dynamic loadlines for bias points ranging from 15 to 40 V at a fixed load impedance of $19 + j16$ is shown in Fig. 5. The loci of the loadlines in the on state suggest that the degradation of PAE is due to a significant rise in R_{on} with increased bias. As can be seen from Fig. 5, this is due to the change in the attainable RF knee voltage past the static bias of $V_D = 25$ V. This walk-out of the knee voltage arises from the lengthening of the gate–drain space–charge region that is controlled by the bias point [15], [16].

This increase in R_{on} can be thought of an additional bias-dependent drain resistance R_{NL} contributing to R_D, as shown in the cross-sectional schematic of Fig. 6. As the dc bias increases, the space charge region between gate and drain increases in size. Due to traps in this high-field region, however, this gate–drain space–charge region cannot respond to microwave frequencies. The result is an increased drain resistance and resultant higher knee voltage during microwave operation.

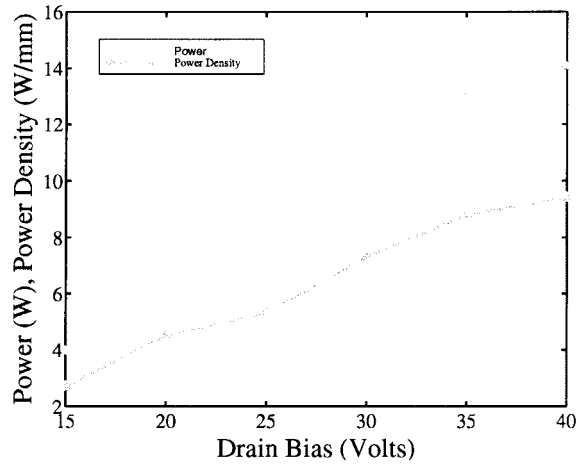

(a)

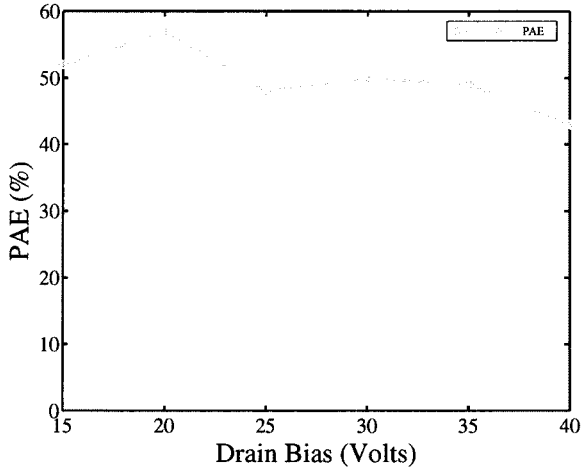

(b)

Fig. 4. (a) Output power/power density. (b) PAE as a function of drain bias for a GaN HEMT at 8 GHz and $V_G = -3.75$ V.

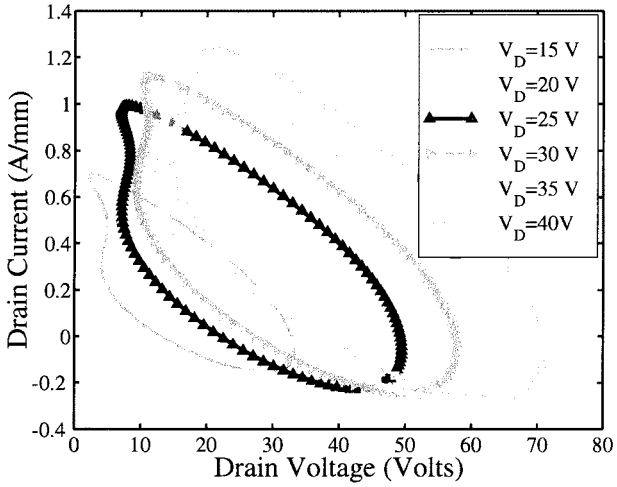

Fig. 5. Dynamic loadlines for $10 \times 150 \times 0.25$ μm^2 AlGaN/GaN HEMT with a fixed load impedance of $19 + j16$ as a function of drain bias under pulsed-biasing conditions with $VG = -3.75$ V at 8 GHz.

VI. Discussion and Conclusion

This paper has used dynamic loadline analysis as a means of understanding the behavior of state-of-the-art AlGaN/GaN HEMTs. It is seen that trap effects cause a discreprancy between the dc *I–V* curves and the realized microwave dynamic loadlines at high drain biases. This limits the performance of the device. This section concludes this paper with a brief discussion of trapping in the device and a comparison of these results with other results for both GaN and GaAs technologies using the Johnson figure-of-merit.

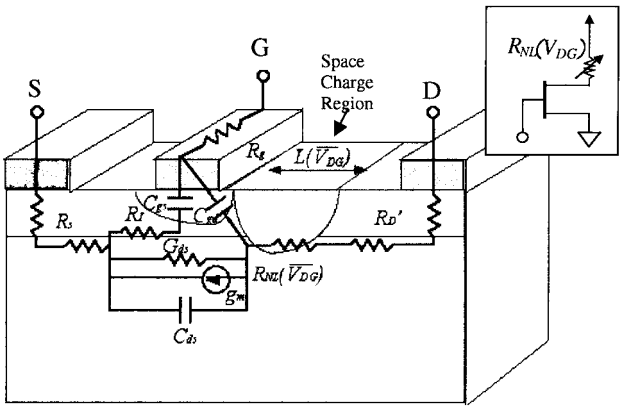

Fig. 6. Schematic illustration of bias-dependent drain-resistance model used to explain the walk-out of knee voltage seen in Figs. 3 and 4.

A. Role of Traps in Limiting Large-Signal Performance

Due to the lack of reproducible lattice-matched substrates and relative immaturity of AlGaN/GaN processing technology, many bulk and surface defects exist in the device material. Bulk traps, due primarily to threading dislocations in the material, reduce the sheet carrier concentration of the device by an amount that depends on the exact dislocation density. This is one reason for the lower current densities observed in AlGaN/GaN HEMTs grown on sapphire substrates. In addition, these bulk traps give rise to "drain lag," which is a source of dispersion in the device output conductance. For the devices considered here, it is held that traps at the surface or possibly in the AlGaN barrier or AlGaN/GaN interface have a more significant impact on large-signal operation.

As alluded to in Section II, surface passivation is essential for obtaining high power densities. Deep level transient spectroscopy (DLTS) studies on similar AlGaN/GaN/SiC HEMTs fabricated at Cornell University, Ithaca, NY, show a very strong peak in the DLTS signal with an associated energy of 1.4 eV prior to passivation. After passivation, the magnitude of the peak at this energy is greatly reduced and the realized microwave power density improves [17]. This suggests that, of the possible trapping mechanisms, those on the surface have the most dominant effect on device performance.

Improved processing such as a gate recess, wherein the gate is placed in a notch, may help improve the situation by moving the channel farther away from the surface. However, such an improvement often reduces the off-state breakdown voltage. It is important to note that no evidence of off-state breakdown-related behavior is seen in the dynamic loadline data presented here. The achievement of even higher output power and PAEs for this technology will depend on a tradeoff between a high breakdown voltage and minimum walk-out of

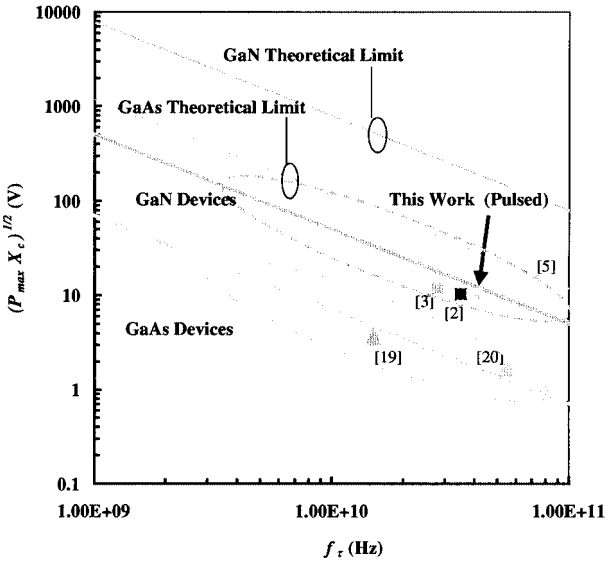

Fig. 7. Comparison of Johnson figure-of-merit for GaAs and GaN device results to theoretical limit (squares are GaN results and triangles are GaAs results).

TABLE I
COMPARISON OF GaAs AND GaN MATERIAL PARAMETERS [1]

Material	E_G (eV)	E_{br} (MV/cm)	v_{sat} (cm/s)
GaN	3.4	3.3	2×10^7
GaAs	1.4	0.4	1.8×10^7

the RF knee voltage. Notwithstanding these nonideal effects, the power results are on par with the state-of-the-art for AlGaN/GaN HEMTs with $>$1-mm gate periphery under pulsed RF measurement conditions.

B. Johnson Figure-of-Merit Assessment of Results

In the final assessment of these results, it is insightful to compare the microwave power performance limits of AlGaN/GaN HEMTs to those of more mature GaAs-based technologies. The Johnson figure-of-merit for power devices [18] gives a comprehensive answer to the question in terms of the *electrical performance* of the devices. An expression for this limit is given by

$$\sqrt{P_{\max} X_c}\, f_\tau \leq E_{br} v_{\text{sat}}/2\pi \tag{4}$$

where $P_{\max}$ is the output power, f_τ is the transit frequency, and X_c is the capacitive input reactance of the device at the frequency at which $P_{\max}$ is measured. This figure-of-merit essentially bounds the watts per unit input capacitance for a given device f_τ by the product proportional to the breakdown field strength of the transistor material and the saturated velocity of the material. This figure-of-merit quantifies the relative ease with which technologies can deliver a specific output power at a given frequency. Fig. 7 compares the Johnson figure-of-merit for state-of-the-art GaN and GaAs power devices to their respective theoretical limits based on the material parameters shown in Table I.

The graph shows large differences between the theoretical limit for GaAs and GaN technologies and the device results for the respective technologies. It is important to note that both GaN and GaAs device technology show a similar gap between the device results and the theoretical maximum for the respective materials. This finding shows how the learning from the development of GaAs-based devices over the last three decades has helped the development of GaN move forward very quickly; work on GaN HEMTs has been largely limited to the last seven years. In spite of this rapid progress, much work still remains to be done for GaN devices in terms of: 1) reducing surface trapping effects through process improvements; 2) understanding the long-term reliability of the devices through increased commercialization efforts; and 3) improving thermal management of large devices through wafer thinning.

In conclusion, this paper has presented 8-GHz dynamic load-line analysis of state-of-the-art 1.5-mm AlGaN/GaN HEMTs under pulsed RF conditions. The measured data have suggested surface trapping as the cause of additional RF on resistance that causes premature gain compression, limiting the realized PAE of the devices. Nonetheless, the pulsed output power density at 8 GHz is unprecedented for competing technologies. Further progress in AlGaN/GaN device fabrication technology will, in the fullness of time, yield even greater performance advantages for the technology.

ACKNOWLEDGMENT

The authors gratefully acknowledge their discussions with Dr. C. E. Weitzel, Motorola Inc., Tempe, AZ. This work was performed at Cornell University, Ithaca, NY, and monitored by Dr. J. Zolper.

REFERENCES

[1] B. E. Foutz, S. K. O'Leary, M. S. Shur, and L. F. Eastman, "Transient electron transport in wurtzite GaN, InN, and AlN," *J. Appl. Phys.*, vol. 85, no. 11, pp. 7727–7734, 1999.

[2] V. Tilak, B. Green, H. Kim, J. Smart, V. Kaper, T. Prunty, J. R. Shealy, and L. F. Eastman, "The influence of barrier thickness on the high power performance of AlGaN/GaN HEMTs," *IEEE Electron Device Lett.*, vol. 48, pp. 504–506, Nov. 2001.

[3]

[4] N. X. Nguyen, M. Micovic, P. Janke, P. Hashimoto, D. W. S. Wong, J. S. Moon, L. McCray, and C. Nguyen, "High performance microwave power GaN/AlGaN MODFET's grown by RF-assisted MBE," *Electron Lett.*, vol. 36, no. 5, pp. 161–163, Mar. 2, 2000.

[5] J. S. Moon, M. Micovic, P. Janke, P. Hashimoto, W.-S. Wong, R. D. Widman, L. McCray, A. Kurdoghlian, and C. Nguyen, "GaN/AlGaN HEMT's operating at 20 GHz with continuous-wave power density $<$6 W/mm," *Electron Lett.*, vol. 37, no. 8, pp. 528–530, Apr. 12, 2001.

[6] C. J. Wei, Y. E. Lan, J. C. M. Hwang, W.-J. Ho, and J. A. Higgins, "Waveform-based modeling and characterization of microwave power heterojunction bipolar transistors," *IEEE Trans. Microwave Theory Tech.*, vol. MTT-43, pp. 2899–2903, Dec. 1994.

[7] M. Demmler, P. J. Tasker, J. G. Leckey, and M. Schlechtweg, "The determination of the transistor dynamic I–V characteristic from large signal RF measurements," in *Proc. 25th Eur. Microwave Conf.*, vol. 1, 1995, pp. 553–557.

[8] L. F. Eastman, V. Tilak, J. Smart, B. M. Green, E. M. Chumbes, R. Dimitrov, H. Kim, O. S. Ambacher, N. Weimann, T. Prunty, M. Murphy, W. J. Schaff, and J. R. Shealy, "Undoped AlGaN/GaN HEMTs for microwave power amplification," *IEEE Trans. Electron Devices*, vol. 48, pp. 479–485, Mar. 2001.

[9] J. A. Smart *et al.*, "AlGaN/GaN heterostructures on insulating AlGaN nucleation layers," *Appl. Phys. Lett.*, vol. 75, pp. 388–390, 1999.

[10] B. M. Green, V. Tilak, S. Lee, H. Kim, J. A. Smart, K. Webb, J. R. Shealy, and L. F. Eastman, "High power broadband AlGaN/GaN MMIC's on SiC substrates," *IEEE Trans. Microwave Theory Tech.*, vol. 49, pp. 2486–2493, Dec. 2000.
[11] B. M. Green, K. K. Chu, E. M. Chumbes, J. A. Smart, J. R. Shealy, and L. F. Eastman, "The role of surface passivation on the microwave characteristics of AlGaN/GaN HEMTs," *IEEE Electron Device Lett.*, vol. 21, pp. 268–270, June 2000.
[12] G. Gonzalez, *Microwave Transistor Amplifiers*. Englewood Cliffs, NJ: Prentice-Hall, 1998.
[13] S. C. Cripps, *Wireless Power Amplifier Design*. Norwood, MA: Artech House, 2000.
[14] V. Kaper, V. Tilak, B. Green, T. Prunty, L. F. Eastman, and J. R. Shealy, "Dependence of power, efficiency and linearity performance of AlGaN/GaN HEMT's on the load resistance for class B bias," in *Proc. IEEE Lester F. Eastman High Performance Devices Conf.* , Newark, DE, Aug. 6–8, 2002, pp. 118–125.
[15] R. Vetury, Y.-F. Wu, P. T. Fini, G. Parish, S. Keller, S. P. DenBaars, and U. Mishra, "Direct measurement of gate depletion in high breakdown (405 V) AlGaN/GaN heterostructure field effect transistors," in *IEEE Electron Devices Meeting Dig.*, 1998, pp. 55–58.
[16] R. Vetury, N. Q. Zhang, S. Keller, and U. Mishra, "The impact of surface states on the DC and RF characteristics of AlGaN/GaN HFETs," *IEEE Trans. Electron Devices*, vol. 48, pp. 560–566, Mar. 2001.
[17] A. V. Vertiatchikh, L. F. Eastman, W. J. Schaff, and T. Prunty, "Effect of surface passivation of AlGaN/GaN heterostructure field effect transistor," *Electron Lett.*, vol. 38, no. 8, pp. 388–389, 19??.
[18] E. O. Johnson, "Physical limitations on frequency and power parameters of transistors," *RCA Rev.*, vol. 26, no. 2, pp. 163–167, 1965.
[19] W. Marsetz, A. Hulsmann, K. Kohler, M. Demmler, and M. Schlechtweg, "GaAs pHEMT with 1.6 W/mm output power density," *Electron Lett.*, vol. 35, no. 9, pp. 748–749, Apr. 29, 1999.
[20] M. Siddiqui, A. K. Sharma, L. G. Callejo, C.-H. Chen, K. Tan, and H.-C. Yen, "A high power and high efficiency power amplifier for local multipoint distribution service," in *IEEE MTT-S Int. Microwave Symp. Dig.*, 1996, pp. 701–704.

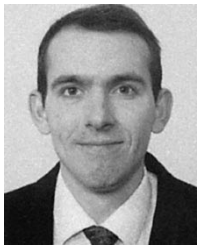

Bruce M. Green (S'96–M'01) received the B.S. and M.S. degrees in electrical engineering (with an emphasis was on electromagnetics and wireless communications handset antennas) from Brigham Young University (BYU), Provo, UT, in 1996 and 1997, respectively, and the Ph.D. degree from Cornell University, Ithaca, NY, in 2001. His doctoral research concerned the characteristics, optimization, and integrated circuit applications of AlGaN/GaN HEMTs.

Upon graduation, he joined the Digital DNA Laboratories, Motorola, where he was involved in the research and development of advanced III–V device technologies. He has authored or coauthored over 20 papers in refereed journals and conference proceedings. He has one patent pending.

Dr. Green is a member of the IEEE Microwave Theory and Techniques Society (IEEE MTT-S), the IEEE Electron Devices Society, Tau Beta Pi, and Eta Kappa Nu. He has served as a reviewer for several IEEE journals. He was the recipient of a 1996–1999 National Science Foundation (NSF) Fellowship, the 1998 IEEE MTT-S Microwave Theory and Techniques Graduate Fellowship, and a 1999 Schlumberger Foundation Fellowship.

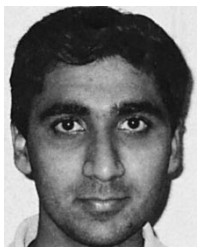

Vinayak Tilak was born in Chennai, India. He received the M.Sc. degree in physics and B.E. degree in electrical engineering from Birla Institute of Technology and Science, Pilani, India, in 1997, and the Ph.D. degree in applied and engineering physics from Cornell University, Ithaca, NY, in 2002.

His research interests include high-frequency devices and circuits and development and modeling of high-power devices on gallium nitride.

Valery S. Kaper (S'97) received the B.S. (*magna cum laude*) and M.S. degrees in electrical engineering from the University of Massachusetts, Lowell, in 1997 and 1999, respectively, and is currently working toward the Ph.D. degree at Cornell University, Ithaca, NY.

From 1995 to 2000, he was with the Semiconductor Device Reliability Group, M/A-COM, Lowell, MA. His research interests are characterization, modeling, and circuit design of AlGaN/GaN HEMTs.

Joseph A. Smart, photograph and biography not available at time of publication.

James R. Shealy, photograph and biography not available at time of publication.

Lester F. Eastman (A'53–M'58–SM'65–F'69–LF'94) is currently the John L. Given Foundation Chair Professor of Engineering at Cornell University, Ithaca, NY. Beginning in 1998, he became devoted full time to graduate research and currently has nine graduate students under his supervision. In 1957, he joined the faculty of electrical engineering at Cornell University. He also serves as a member of the graduate fields of applied physics and materials science. Since 1965, he has conducted research on compound semiconductor materials and high-speed devices and circuits, and has been active in organizing workshops and conferences on these subjects elsewhere since 1965 and at Cornell University since 1967. In 1977, he joined other Cornell University faculty members in obtaining funding and founding the National Research and Resource Facility for Submicron Structures at Cornell (now Cornell Nanofabrication Facility). Also in 1977, he founded the Joint Services Electronics Program and directed it until 1987. He has supervised over 100 Ph.D. dissertations, over 50 M.S. theses, and over 50 post-doctoral studies. In his research group, effort is underway on molecular beam epitaxy, microwave transistors, high-speed semiconductor lasers, and fundamental phenomena in compound semiconductor quantum electron and optical devices. From 1978 to 1979, he was on leave at the Massachusetts Institute of Technology (MIT) Lincoln Laboratory, and from 1985 to 1986, he was with the IBM Watson Research Laboratory. He has served as a consultant for several industries.

Dr. Eastman is a member of the National Academy of Engineering (since 1986) and was appointed the John L. Given Foundation Chair Professor of Engineering at Cornell University in January 1985. In 2001, he became a Fellow of the American Physical Society. During 1983, he was the IEEE Electron Device Society National Lecturer. He was a member of the U.S. Government Advisory Group on Electron Devices from 1978 to 1988. From 1987 to 1993, he served as a member of the Kuratorium (Visiting Senior Advisory Board) of the Fraunhofer Applied Physics Institute, Freiburg, Germany. He was the recipient of the 1991 GaAs Symposium Award and the Heinrich Welker Medal for his "contributions to the development of ballistic electron devices, planar doping, buffer layers, and Al1nAs/GaInAs/InP heterostructures." He was also the recipient of the 1994 Alexander von Humboldt Senior Fellowship and the 1995 Aldert van der Ziel Award. He was the recipient of the 1999 IEEE Graduate Teaching Award, the 2000 IEEE Third Millennium Medal, and the 2002 J. J. Ebers Award of the IEEE Electron Device Society.